



Reaction Mechanism of the Metal Precursor Pulse in Plasma-Enhanced Atomic Layer Deposition of Cobalt and the Role of Surface Facets

Liu, J., Lu, H., Zhang, D. W., & Nolan, M. (2020). Reaction Mechanism of the Metal Precursor Pulse in Plasma-Enhanced Atomic Layer Deposition of Cobalt and the Role of Surface Facets. *Journal Of Physical Chemistry C*, 124(22), 11990-12000. <https://doi.org/10.1021/acs.jpcc.0c02976>

[Link to publication record in Ulster University Research Portal](#)

Published in:
Journal Of Physical Chemistry C

Publication Status:
Published (in print/issue): 15/05/2020

DOI:
[10.1021/acs.jpcc.0c02976](https://doi.org/10.1021/acs.jpcc.0c02976)

Document Version
Author Accepted version

General rights
Copyright for the publications made accessible via Ulster University's Research Portal is retained by the author(s) and / or other copyright owners and it is a condition of accessing these publications that users recognise and abide by the legal requirements associated with these rights.

Take down policy
The Research Portal is Ulster University's institutional repository that provides access to Ulster's research outputs. Every effort has been made to ensure that content in the Research Portal does not infringe any person's rights, or applicable UK laws. If you discover content in the Research Portal that you believe breaches copyright or violates any law, please contact pure-support@ulster.ac.uk.

Reaction Mechanism of the Metal Precursor Pulse in Plasma-Enhanced Atomic Layer Deposition of Cobalt and the Role of Surface Facet

Ji Liu^a, Hongliang Lu^b, and David Wei Zhang^b, Michael Nolan^{a,*}

^a Tyndall National Institute, University College Cork, Lee Maltings, Dyke Parade, Cork, T12 R5CP, Ireland

^b State Key Laboratory of ASIC and System, Shanghai Institute of Intelligent Electronics & Systems, School of Microelectronics, Fudan University, Shanghai 200433, China

Corresponding author:

*E-mail: Michael.nolan@tyndall.ie. Tel: +353 021 2346983

Abstract

Cobalt is a potential candidate in replacing copper for interconnects and has been applied in the trenches and vias in semiconductor industry. A non-oxidizing reactant is required in plasma-enhanced atomic layer deposition (PE-ALD) of thin films of metals to avoid O-contamination. PE-ALD of Co has been demonstrated experimentally, but the growth mechanism and key reactions are not clear. In this paper, the reaction mechanism of metal cyclopentadienyl (Cp, C_5H_5) precursors ($CoCp_2$) and NH_x -terminated Co surface is studied by density functional theory (DFT) calculations. The Cp ligands are eliminated by CpH formation via a hydrogen transfer step and desorb from metal surface. The surface facet plays an important role in the reaction energies and activation barriers. The results show that on the NH_x -terminated surfaces corresponding to ALD operating condition (temperature range 550K to 650K), the two Cp ligands are eliminated completely on Co(100) surface during the metal precursor pulse, resulting in Co atom deposited on the Co(100) surface. But the second Cp ligand reaction of hydrogen transfer is thermodynamically unfavourable on the Co(001) surface, resulting in CoCp fragment termination on Co(001) surface. The final terminations after metal precursor pulse are 3.03 CoCp/nm^2 on NH_x -terminated Co(001) surface and 3.33 Co/nm^2 on NH_x -terminated Co(100) surface. These final structures after metal precursor pulse are essential to model the reaction during the following N-plasma step.

1. Introduction

Copper (Cu) has been widely used in the semiconductor industry as interconnect for 20 years.¹ However, continuous deposition of Cu films needed for interconnect in nanoelectronics is difficult and a barrier layer is required to prevent the diffusion of Cu into the dielectric layer and Si substrates. Cu also aggregates into 3D structures.²⁻³ Finding suitable barrier/liner layer is still a challenge because issues with copper reduce the electrical resistivity of the interconnect, especially for devices at nanosize dimension. One solution is to replace Cu with metals that do not suffer these issues. Transition metal Cobalt (Co) is important as candidates in replacing Cu for interconnects and has been applied in the trenches and vias with the downsizing of semiconductor devices.⁴⁻⁶ There is also the question of deposition of nanoscale films, in particular on high aspect ratio structures, where different surface facets maybe present. Atomic layer deposition (ALD) is applied for conformal deposition and growth control at the atomic level, which is needed for deposition onto high aspect ratio structures.⁷⁻⁸ Generally, ALD consists of two self-limiting half cycles, where the reactions will stop after all available surface sites are consumed. In addition to the successful application of ALD in microelectronics and the semiconductor industry, it is further applied in the areas of catalysis and energy conversion and storage.^{5, 9-10}

For the ALD of Co, Cp based precursors such as CoCp_2 , $\text{CoCp}(\text{CO})_2$ and $\text{Co}(\text{CpAMD})$ have been developed and applied.¹¹⁻¹² For thermal ALD of Co with metal precursor and hydrogen reactant, the required growth temperature can be as high as 350°C , but the growth rate is as low as $0.12 \text{ \AA}/\text{cycle}$.¹³ With the application of plasma-enhanced ALD (PE-ALD), the temperature can be reduced to 75°C . The reported growth cycle with CoCp_2 is increased to $1.5 \text{ \AA}/\text{cycle}$.¹⁴⁻¹⁵ For the N-plasma source, a mixture of N_2 and H_2 is used and the properties of the deposited Co thin film greatly depend on the N_2/H_2 gas flow ratio.¹⁶⁻¹⁷ It is noted that H_2 plasma alone or individual N_2

and H₂ plasma results in high resistivity and low purity Co thin films. Previous studies argue that the presence of NH_x species is needed to deposit low resistivity and high purity Co thin film.¹⁸ NH_x species are needed for chemisorption of metal precursor and removal of the Cp ligand. But they are not incorporated in the film, because most of the N may desorb in the form of either NH₃ or N₂. The detailed mechanism requires deeper study, but one possible reason is that highly reactive radicals from N-plasma source should be present for successful PE-ALD of Co. The final structure and termination after the metal precursor pulse are vital and essential to model the plasma step, which is the key advance of current paper.

Density functional theory (DFT) calculations have been successfully applied to study the ALD of metals and metal oxides.¹⁹⁻²² Theoretically, the design and large-scale screening of precursors based on specific criteria such as the thermodynamic stability and kinetic stability have been performed in ALD modelling.²³⁻²⁴ DFT calculations can also be applied to reveal the reaction mechanisms and the derived growth rate serves as guideline to experiments. In the early stage, the deposition of metal oxide, such as Al₂O₃ from trimethylaluminum and O₃/H₂O as the co-reactant, has been studied theoretically.²⁵⁻²⁹ The surface hydroxyl groups are formed and their surface coverages affect the growth rate. For the deposition of metals, Elliott has proposed a mechanism for deposition of noble metals including Pd, Ir and Pt using homoleptic precursors and oxygen from DFT calculations.³⁰ It is found that each ligand is replaced by a hydroxyl group, which can be further eliminated by Brønsted-type reaction.

The reaction mechanism using oxidizing reactant such as O₃ and H₂O is well-established. However, when depositing metals, O-source can promote oxidation of the metal surface and therefore cause contamination. Non-oxidizing reactants such as NH₃ in PE-ALD of transition metals have been experimentally developed. A complete PE-ALD process using N-plasma is as

follows. Firstly, it is vital to note that at the post-plasma stage, the metal surface is actually the NH_x -terminated metal surface. In the first half-cycle, the metal precursor CoCp_2 reacts with NH_x -terminated metal surface. The Cp ligand is eliminated by hydrogen transfer from the surface to form CpH , which desorbs from surface. In the second half-cycle, the plasma generated radicals such as N_xH_y will react with the precursor fragment terminated metal surface and the Co atoms are deposited on the surface, which is covered by NH_x groups at the end of second half cycle. In our recent published work, the nature and stability of NH_x -terminated metal surfaces were studied.³¹ The results show that at ALD operating condition (temperature range 550K to 650K), on the low energy (001) surface, NH-termination is the most stable surface termination, while on the high energy (100) surface, a mixture of NH and NH_2 is the most stable surface termination.

In this paper, we explore the reaction mechanism for the metal precursor pulse by DFT calculations. The elimination of Cp ligand is the key step during the metal precursor pulse. Single metal precursor CoCp_2 is adsorbed on the NH_x -terminated surfaces³¹ and the hydrogen transfer step is studied in detail with calculation of proton migration barrier. After the first CpH formation and desorption, the possibility of the loss of second Cp ligand is also investigated. With the NH_x terminations at ALD operating condition, on the Co(100) surface, the metal precursor can undergo two hydrogen transfer steps and the two Cp ligands are eliminated completely, resulting in Co atom deposition on the surface, binding to N atom. However, only one Cp ligand is eliminated on the Co(001) surface, resulting in CoCp fragments on the surface after the metal precursor pulse. The precursor coverage effect is studied with two metal precursors CoCp_2 adsorbed on the surface. A neighbouring CoCp has hindered the reactivity by increasing the activation barrier of the first hydrogen transfer on Co(001) surface, but promoted the reactivity by lowering the activation barrier of the first hydrogen transfer on Co(100) surface. The determined surface coverage of final

terminations after the metal precursor pulse are 3.03 CoCp/nm² on NH_x-terminated Co(001) surface and 3.33 Co/nm² on NH_x-terminated Co(100) surface.

2. Methods and Computational Details

All the calculations are performed on the basis of periodic spin-polarized density functional theory (DFT) within a plane wave basis set and projector augmented wave (PAW) formalism³², as implemented in the Vienna *ab initio* simulation package (VASP 5.3) code. The generalized gradient approximation (GGA) with the parameterization of Perdrew-Burke-Ernzerhof (PBE) is used for the exchange-correlation functional.³³⁻³⁴ We use 9 valence electrons for Co, 5 for N, 4 for C, and 1 for H. The plane wave energy cutoff is set to be 400eV. The convergence of energy and forces are set to be 1×10⁻⁴eV and 0.01eV/Å, respectively. The bulk Co crystal structure is optimized by simultaneously relaxing the ionic positions, cell volume and cell shape at a higher plane wave energy cutoff of 550eV and using a Monkhorst-Pack grid k-point mesh³⁵ of 12 × 12 × 6. The resulting lattice constants are a = b = 2.49Å, and c = 4.03Å for Co bulk.

The deposited Co films by PE-ALD are polycrystalline and have random surface orientations after low temperature deposition. Based on our previous study³¹ on the stability of NH/NH₂ terminations, we have chosen the most stable (001) surface and a less stable but high reactivity surface, namely (100), to investigate the precursor reaction mechanism. A (4×4) supercell is used to model the (001) surface with a surface lattice of a = b = 9.96Å (surface area = 0.99 nm²), while a (3×3) supercell, with a surface lattice of a = 7.47Å, b = 12.10Å (surface area = 0.90 nm²), is used to model the (100) surface. For the Co(001) surface, a five-layer slab is used, with the bottom three layers fixed during the calculation; while for the Co(100) surface, due to zigzag structure, a four-bilayer (eight atomic layer) slab is built with the bottom two bilayers (bottom four layers) fixed during the calculations. From our previous studies, fixing these-layers is sufficient to model these

Co surfaces.³¹ A k-point mesh³⁵ of $2 \times 2 \times 1$ is used in (4×4) supercell and for the (3×3) supercell a $3 \times 2 \times 1$ mesh is used.

Our previous DFT study³¹ of NH_x saturation coverage shows that at zero-K condition, the Co(001) surface is terminated with 0.67ML NH and 0.23ML NH_2 , which contains 10 NH and 4 NH_2 in a (4×4) supercell. On the Co(100) surface, the termination is 1ML NH and 1ML NH_2 due to the trench structure, which contains 9 NH and 9 NH_2 in (3×3) supercell. The saturation coverages are summarized in Table 1. The configurations of the NH_x -terminated Co surfaces at zero-K condition are shown in Figure 1(a)-(b).

Table 1. The calculated saturation coverages on Co (001) and (100) surfaces at zero-K and ALD conditions.

	Co(001)	Co(100)
	(4×4)	(3×3)
Zero-K condition	0.67ML NH + 0.23ML NH_2	1ML NH + 1ML NH_2
ALD condition	0.56ML NH	0.67ML NH + 0.67ML NH_2

At ALD operating condition (temperature range 550K to 650K), some of the surface NH_x species desorb from the surface. The preferred NH_x coverages are³¹: Co(001) surface is terminated with 0.56ML NH, which is 9 NH in (4×4) supercell. On the Co(100) surface, the preferred surface termination is 0.67ML NH and 0.67ML NH_2 , which contains 6 NH and 6 NH_2 in (3×3) supercell. The configurations of NH_x terminations Co surfaces at the ALD operating condition are shown in Figure 1(c)-(d). On the (100) surface, due to the trench structure, NH prefers the subsurface

channel bridge site and NH_2 prefers the surface bridge site. The channel bridge is a bridge site with two channel metal atoms and the surface bridge is the bridge site with two surface metal atoms. The configuration of single NH and NH_2 adsorbed on channel bridge and surface bridge sites is shown in Figure S1 in the supporting information.

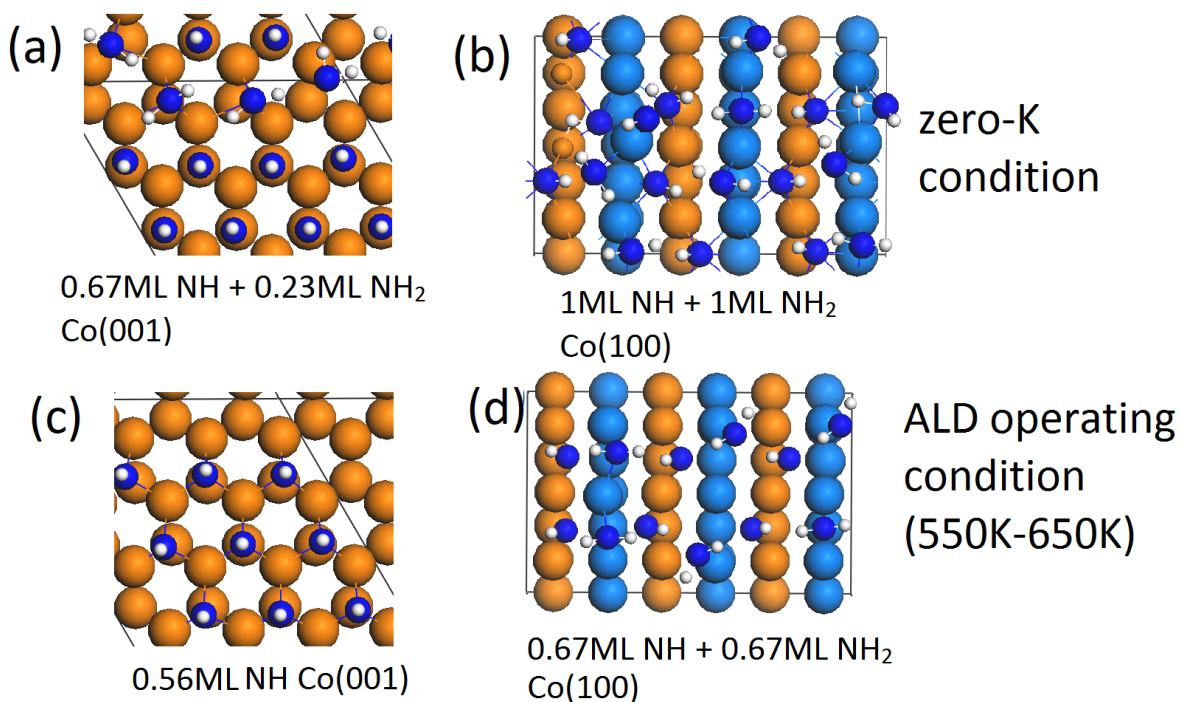


Figure 1. The top view of NH_x terminated metal surfaces at zero-K condition including (a) Co(001), and (b) Co(100) and at ALD operating condition including (c) Co(001), and (d) Co(100). Co atom is represented by orange for surface terminating atoms and light blue for the channel bridge subsurface atoms in the (100) surface; N atom and H atom are represented by dark blue and white atom, respectively.

The molecular geometries of the metal precursor CoCp₂ are relaxed in the same supercell as Co(001), with an energy cutoff of 400eV and Gamma point sampling. The van der Waals correction is applied with the PBE-D3 method to ensure an accurate description of the metal precursor adsorption energy.³⁶ The activation barriers reported in this paper are computed using climbing image nudged elastic band (CI-NEB) method³⁷ with 6 images including the starting and ending geometries and with the forces converged to 0.05eV/Å.

3. Results and Discussions

3.1 Metal precursor adsorption on NH_x-terminated Co (001) and (100) surfaces

The structure of the gas phase metal precursor is first described. For CoCp₂, the Cp-Cp distance is between 3.39Å to 3.40Å. The Co-C distance is between 2.08Å to 2.10Å, indicating little tilting of the two Cp rings. When adsorbed on the NH_x-terminated metal surfaces, the metal precursor can be placed perpendicular to substrate with one Cp ring interacting with the surface (the **upright** position) or parallel to surface with both Cp rings interacting with the surface (the **flat** position). The adsorption energy is calculated from:

$$E_{ad} = E_{tot} - E_{\frac{NH_x}{Metal}} - E_A \quad (1)$$

where E_{tot}, E_{NH_x/Metal}, and E_A are the energy of the NH_x-terminated metal slab with adsorbed precursor CoCp₂, the slab model for the NH_x-terminated metal surface, and the isolated CoCp₂ precursor, respectively. All the energies are computed with the van der Waals correction included. A negative adsorption energy corresponds to exothermic adsorption. We will use the NH_x coverages obtained at zero K and ALD conditions to explore the effect of NH_x coverage on the CoCp₂ pulse.

3.1.1 Metal precursor adsorption on NH_x-terminated Co (001) and (100) surfaces at high coverage

The calculated adsorption energies of the metal precursors on NH_x-terminated Co (001) and (100) surfaces at maximum NH_x coverage (Table 1) are shown in Table 2. Co(001) is terminated with 0.67NL NH and 0.23ML NH₂ and Co(100) has mixed termination with 1ML NH and 1ML NH₂. On the (001) surface, the metal precursor prefers to bind to the substrate in the upright adsorption mode through one Cp ring. On the (100) surface, the metal precursor prefers to bind to the substrate through both Cp rings with the precursor in the flat configuration. These structures are shown in Figure 2(a)-(b). The configurations of the corresponding less stable adsorption structures are shown in Figure 2(c)-(d).

Table 2. The calculated adsorption energy of metal precursor CoCp₂ adsorbed on NH_x-terminated Co (001) and (100) surfaces. The NH/NH₂ terminations correspond to the maximum NH_x coverage.

	Co(001)	Co(100)
upright	-0.10	-1.41
flat	3.16	-1.73

This difference in preferred binding mode at the two surface facets is due to the different surface structures. The (001) surface has a flat surface structure, while (100) surface has a unique zigzag structure. On the (001) surface, an upright position with one Cp ring close to metal surface results in stronger adsorption strength as this will maximise the number of interactions between the

surface and carbon of the Cp ring. By contrast, the flat CoCp₂ structure on (001) does not allow carbon-surface interactions and therefore the interaction is less favourable. In addition, in the upright binding mode, each carbon atom in the Cp ring is available for the hydrogen transfer step to form CpH. On Co (001), the distances between the two Cp rings in the upright structure elongate to 3.43 Å, while the metal-C distances elongate to 2.11 Å for the Cp ring interacting with the surface, which is a small elongation compared to the free precursor.

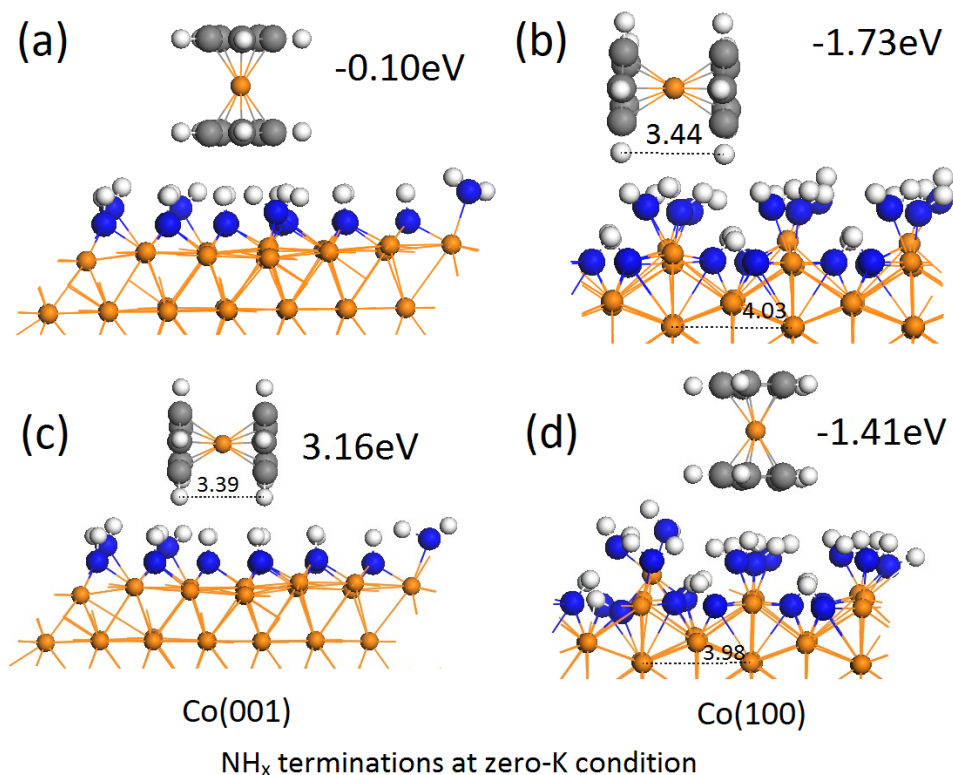


Figure 2. The configurations of the most stable adsorption of precursor CoCp₂ on (a) Co(001) surface, and (b) Co(100) surface and the less stable adsorption of precursor CoCp₂ on (c) Co(001) surface, and (d) Co(100) surface. The NH_x termination is with respect to zero-K condition. Co atoms are represented by orange spheres; Carbon, nitrogen and hydrogen atoms are represented by grey, blue and white colour, respectively.

On the Co (100) surface, the distance across the trench (between two neighbouring surface metal atoms) is 4.03Å. The distances between the two Cp rings in flat configuration are in the range of 3.34Å to 3.44Å and the metal-C distances are 2.07Å to 2.10Å. The metal precursor can therefore be well-accommodated within the trench structure of the Co(100) surface, which promotes the adsorption of the precursor, as indicated by the computed adsorption energies. Compared to free metal Cp precursors, the two Cp rings are tilted with shorter ring-ring distance for the atoms away from the surface and longer ring-ring distance for the atoms closer to the surface.

3.1.2 Metal precursor adsorption on NH_x-terminated Co (001) and (100) surfaces at low NH_x coverage, corresponding to the ALD operating condition

The calculated adsorption energies of the metal precursors on the NH_x-terminated Co (001) and (100) surfaces corresponding to the lower NH_x coverage and the ALD operating condition are shown in Table 3. The initial NH_x terminations are now 0.56ML NH on Co(001) and the mixed termination with 0.67ML NH and 0.67ML NH₂ on Co(100).

Table 3. The calculated adsorption energy of metal precursor RuCp₂ and CoCp₂ adsorbed on (001) and (100) surfaces. The NH/NH₂ terminations corresponds to ALD operating condition (temperature range 550K - 650K).

	Co(001)	Co(100)
upright	-0.68	-0.34
flat	-0.56	-1.67

The binding preference of CoCp₂ is the same as the higher NH_x coverage surfaces and the relaxed adsorption structures are shown in Figure 3(a)-(b). The configurations of less stable adsorption structures are shown in Figure 3(c)-(d). On Co(001) surface, an upright position with one Cp ring close to metal surface can result in stronger adsorption strength, although the flat adsorption mode is now much more favourable compared to the same adsorption mode at higher NH_x coverage. The distances between the two Cp rings are in the range of 3.37Å to 3.40Å on Co(001) surface. Compared with free CoCp₂, the two Cp rings are slightly tilted. The distances for metal-C are between 2.08Å and 2.10Å.

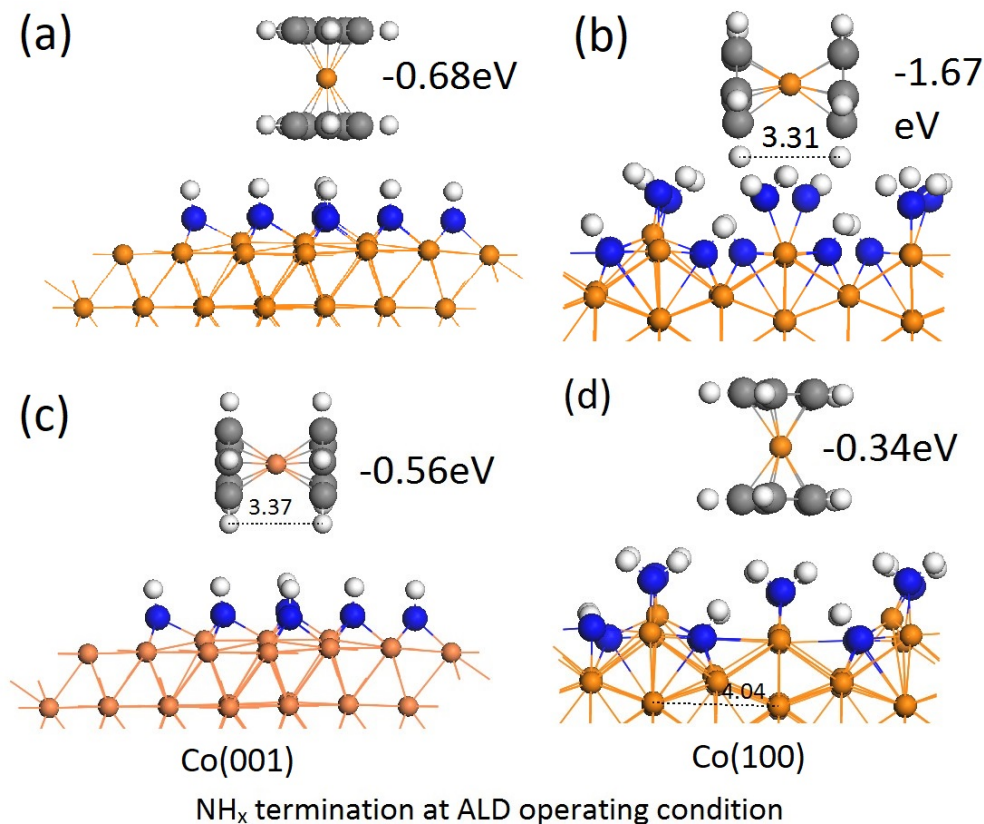


Figure 3. The configurations of the most stable adsorption of precursor CoCp_2 on (a) $\text{Co}(001)$ surface, and (b) $\text{Co}(100)$ surface and the less stable adsorption pf precursor CoCp_2 on (c) $\text{Co}(001)$ surface, and (d) $\text{Co}(100)$ surface. The NH_x termination is with respect to ALD operating condition. Co atoms are represented by orange spheres; Carbon, nitrogen and hydrogen atoms are represented by grey, blue and white colour, respectively.

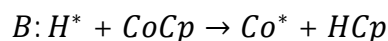
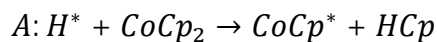
The distance across the trench between two neighbouring metal atoms is 4.03\AA on $\text{Co}(100)$ surface. The distances between the two Cp rings are in the range of 3.31\AA to 3.40\AA . The distances for metal-C are 2.06\AA to 2.10\AA . The flat adsorption mode of metal precursor can be well-accommodated within the trench of the (100) surfaces, which can result in stronger adsorption strength. Compared to free metal Cp precursors, the two Cp rings are tilted with shorter ring-ring

distances for the atoms closer to the surface and longer ring-ring distances for the atoms away from the surface.

3.2 Single precursor reaction pathway on Co (001) and (100) surfaces with NH_x terminations at ALD operating condition

The reaction pathway during the metal precursor pulse is studied with respect to the NH_x terminations at ALD operating condition. In this section, we address the reaction mechanism when a single CoCp₂ precursor is adsorbed on NH_x-terminated Co (001) and (100) surfaces. Once the metal precursor is adsorbed on NH_x-terminated metal surfaces, the Cp ligand can undergo hydrogen transfer, CpH formation, CpH desorption, second hydrogen transfer, and second CpH formation and desorption.

Upon adsorption, no spontaneous hydrogen transfer was observed on any NH_x-terminated Co (001) and (100) surfaces. This means that the hydrogen transfer step must overcome an activation barrier. The possible reactions of a single adsorbed molecule of CoCp₂ on NH_x terminated metal surfaces can be illustrated as follows:



where reaction A involves the first Cp ligand and reaction B involves the second Cp ligand. We have calculated the energy along the reaction pathway and the activation barriers for hydrogen transfer at each step. Note that the reaction energies of precursor adsorption ($E_{\text{adsorption}}$) and the first hydrogen transfer (E_{hydrogen}^I) are with reference to the NH_x-terminated metal surface and free

CoCp₂. If one CpH molecule desorbs from the surface, the reaction energies of first CpH desorption ($E^{\text{Des}}_{\text{CpH}^{\text{I}}}$), second hydrogen transfer ($E_{\text{hydrogen}^{\text{II}}}$), and second CpH desorption ($E^{\text{Des}}_{\text{CpH}^{\text{II}}}$) are with reference to NH_x-terminated metal surface with adsorbed CoCp₂, and free CpH.

The results for NH_x terminations at ALD operating condition are summarized in Figure 4 and the calculated barriers for the hydrogen transfer steps are presented in Table 4. In order to assess any role of NH/NH₂ coverage, the results for NH_x terminations at highest coverage, i.e. zero K, are summarized in Figure S2 and the calculated barrier for the hydrogen transfer steps are presented in Table S1 in supporting information.

Table 4. The calculated reaction energy for hydrogen transfer step and reaction barriers, E_{barrier} , on Co (001) and (100) surfaces with NH_x terminations corresponding to ALD operating condition. $E_{\text{adsorption}}$ is the energy change upon precursor adsorption, $E_{\text{hydrogen}^{\text{I}}}$ and $E_{\text{hydrogen}^{\text{II}}}$ are the energy change for the first and second hydrogen transfer, and $E^{\text{Des}}_{\text{CpH}^{\text{I}}}$ is the desorption energy of CpH.

	$H^* + \text{CoCp}_2 \rightarrow \text{CoCp}^* + \text{HCp}$			$H^* + \text{CoCp} \rightarrow \text{Co}^* + \text{HCp}$		
	$E_{\text{adsorption}}$	$E_{\text{hydrogen}^{\text{I}}}$	E_{barrier}	$E^{\text{Des}}_{\text{CpH}^{\text{I}}}$	$E_{\text{hydrogen}^{\text{II}}}$	E_{barrier}
Co(001)	-0.68	-0.63	0.56	-1.69	-0.72	1.57
Co(100)	-1.67	-2.19	0.52	-1.32	-1.15	0.85

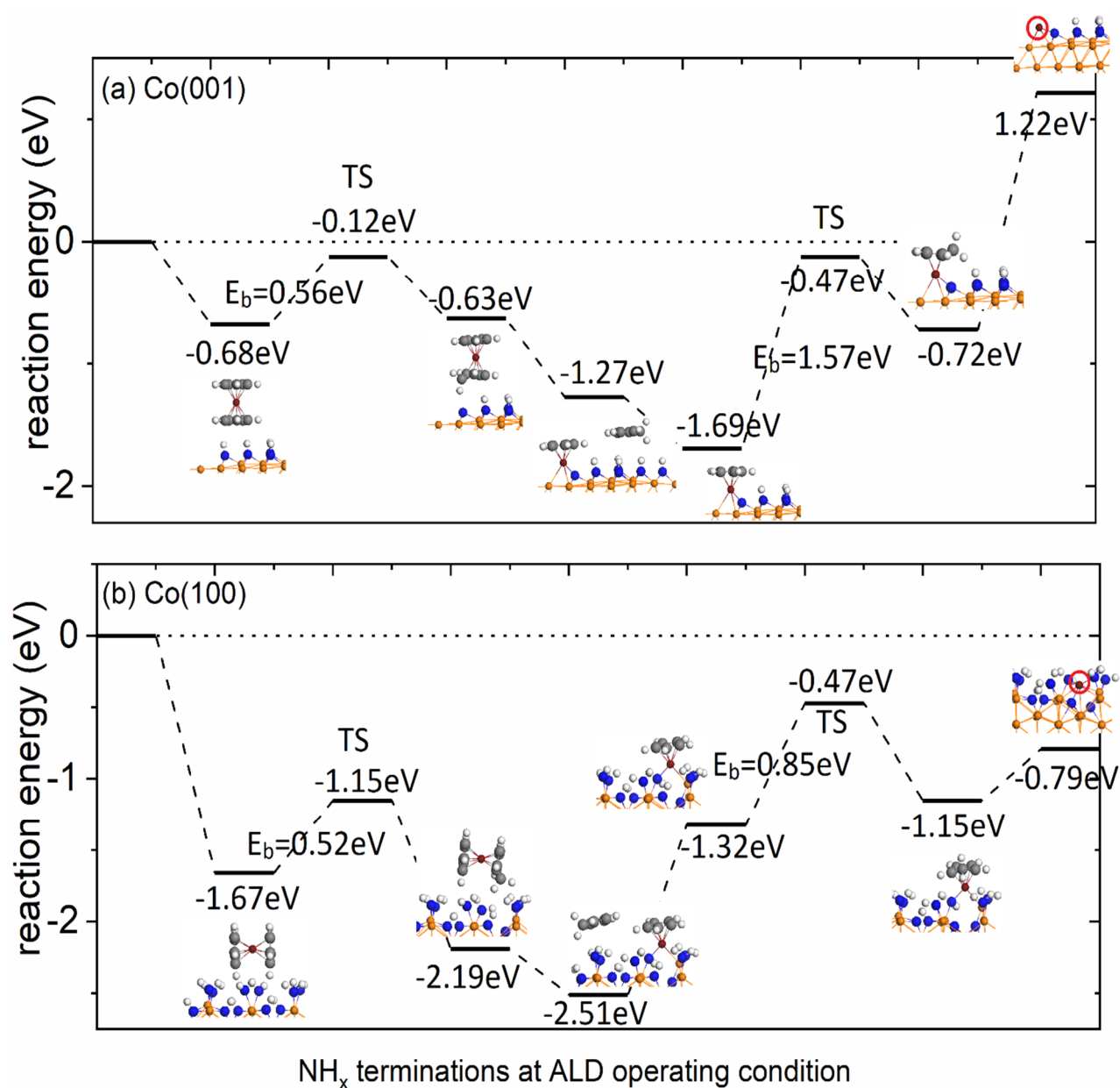


Figure 4. The plotted metal precursor reaction pathway on (a) Co(001) surface and (b) Co(100) surface with NH_x terminations at ALD operating condition. The Cp ligand is eliminated via hydrogen transfer. The substrate Co atoms are represented by orange spheres and the Co atom from CoCp₂ is represented by a red colour. Carbon, nitrogen and hydrogen atoms are represented by grey, blue and white colour, respectively.

On the Co(001) surface, the metal precursor CoCp₂ has a moderate adsorption strength ($E_{\text{adsorption}} = -0.68\text{eV}$). The first Cp ligand elimination via hydrogen transfer is thermoneutral with a moderate barrier of 0.56eV for transfer of hydrogen and a small energy change of 0.05eV. The formation and desorption of this CpH are exothermic and the elimination of this CpH makes the reaction exothermic with a total energy gain of -1.69eV.

Considering now the elimination of the second Cp ligand via hydrogen transfer is highly endothermic with a high activation barrier for hydrogen transfer, which is 1.57eV. The desorption of the second CpH to give a bare Co species that is bound to surface N atom is thermodynamically unfavourable. Thus, the final termination is a CoCp termination on Co(001) as a result of the high barrier and endothermic reaction for the elimination of the second Cp ligand.

At the highest NH_x coverage, the terminations on Co(001) are 0.67ML NH and 0.23ML NH₂. As shown on Figure S2(a) in supporting information, the overall reactions for Cp ligand eliminations via hydrogen transfer step are exothermic. The calculated barriers are 1.00eV and 1.24eV for first and second hydrogen transfer steps. However, the initial adsorption of metal precursor CoCp₂ is quite weak, which has the value of -0.10eV, so that this reaction is not likely to proceed.

On the Co(100) surface, we find that for the hydrogen transfer step, the channel H atom is more reactive than the surface H atom. Table 5 compares the energies for transfer of these two hydrogen species. On the Co(100) surface, after relaxation, a channel hydrogen atom migrates to the surface N atom that has lost hydrogen and this recovers to form NH₂. Thus, in the subsequent discussion of hydrogen transfer on the Co(100) surfaces, the channel H is the active species for hydrogen transfer to the Cp ligand.

Table 5. The calculated reaction energy for hydrogen transfer step from surface H and channel H on Co(100) surface. The results for transfer of different H species show that channel H is more reactive than surface H on the Co(100) surface.

	High NH _x Coverage	ALD Coverage
	Co(100)/eV	Co(100)/eV
Adsorption	-1.73	-1.67
hydrogen transfer channel H	-3.12	-2.19
hydrogen transfer surface H	Recover to NH ₂	Recover to NH ₂

The reaction pathway on Co(100) surface is shown in Figure 4(b). The reaction energies for all steps are exothermic, so that the loss of two Cp ligands as CpH via hydrogen is overall exothermic by -0.79eV. The CoCp₂ precursor initially adsorbs on the NH_x terminated Co(100) surface with a gain of -1.67eV. The first hydrogen transfer step is exothermic, with a moderate activation barrier of 0.52eV and a gain of -0.52 eV in energy. After the first Cp ligand desorption, the second hydrogen transfer step is practically thermoneutral with a moderate barrier of 0.85 eV and a small energy cost of 0.17eV. Finally, the desorption of the second CpH shows an energy gain of -0.79eV and the resulting surface structure shows a Co atom which binds to a nitrogen atom from which a H atom transferred to Cp.

At the highest NH_x coverage, the terminations on Co(100) are 1ML NH and 1ML NH₂. As shown on Figure S2(b) in supporting information, the overall reaction for Cp ligand eliminations via hydrogen transfer step is exothermic. The calculated barriers for the first and second hydrogen

transfer steps are 1.56 eV and 0.84 eV. However, the first CpH formation is endothermic with a high energy cost of 2.82eV. This is due to very strong adsorption of CoCp_2H on the $\text{Co}(100)$ surface after the hydrogen transfer step, which had an energy gain of -3.12eV. Thus, with the highest NH_x coverage, the precursor is too strongly bound to the substrate.

To summarize, for NH_x terminations of Co (001) and (100) at typical ALD operating conditions, at least one Cp ligand can be eliminated *via* a hydrogen transfer step. On the $\text{Co}(001)$ surface, the activation barriers are 0.56eV and 1.57eV for the first and second hydrogen transfer steps. Due to high barrier and endothermic reaction, the elimination of second Cp ligand is unfavourable and the termination for a single $\text{Co}(\text{Cp})_2$ precursor is a CoCp fragment on NH_x terminated $\text{Co}(001)$ surface. On the $\text{Co}(100)$ surface, the activation barriers for the first and second hydrogen transfer steps are 0.52eV and 0.85eV, which would be easily overcome at typical ALD conditions. The two Cp ligands are eliminated and the final desorption of CpH shows an energy gain of -0.79eV. The resulting surface termination after reaction of a single precursor is a Co atom deposited on NH_x terminated $\text{Co}(100)$ surface, which binds to surface N atom. The distance between the deposited Co atom and nearest N atom is 1.84Å. These structures are shown in Figure 5. Not only the NH_x coverage, but also the surface facet play a crucial role in the adsorption strength of the precursor and the energetics of the hydrogen transfer and CpH formation and removal steps.

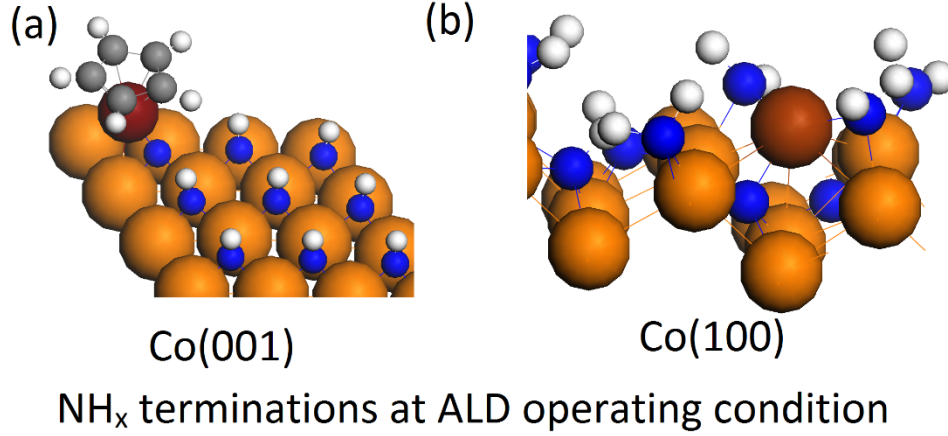


Figure 5. The configurations of the final structures after single metal precursor CoCp₂ adsorption and ligand elimination on the (a) Co(001) and (b) Co(100) surface. The NH_x terminations are at ALD operating condition. The substrate Co atom is represented by orange colour and the Co atom from metal precursor CoCp₂ is represented by wine red colour. Carbon, nitrogen and hydrogen atoms are represented by grey, blue and white colour, respectively.

3.3 Precursor coverage effect on the reaction mechanism on Co (001) and (100) surfaces with NH_x terminations at ALD operating condition

We now address the adsorption and further reaction of two Co(Cp)₂ precursors. The adsorption energy is calculated from:

$$E_{ad} = E_{tot} - E_{\frac{NH_x}{Metal}} - 2 * E_A \quad (2)$$

where E_{tot} , $E_{NH_x/Metal}$, and E_A are the energy of the NH_x-terminated metal slab with two precursor CoCp₂, the slab model for the NH_x-terminated metal surface, and isolated precursor CoCp₂, respectively. Dividing the computed energy by two gives the adsorption energy per precursor. All energies are computed with the inclusion of the van der Waals corrections. The adsorption

structures of two precursors on Co (001) and (100) surfaces at the ALD coverage of NH_x are shown in Figure 6.

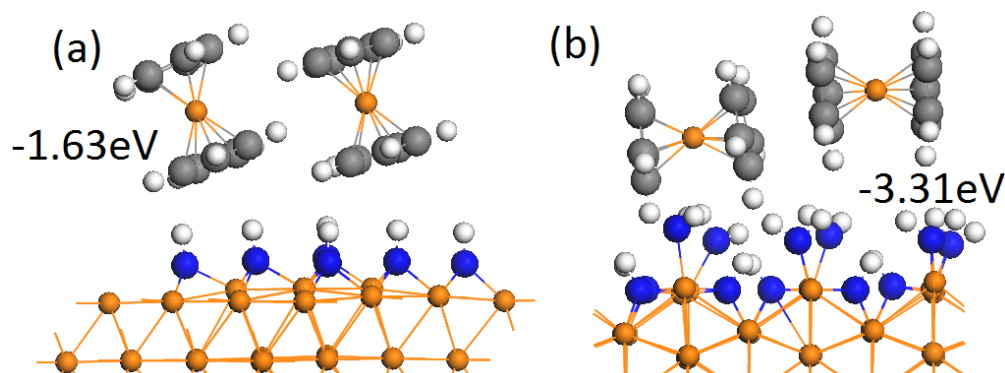
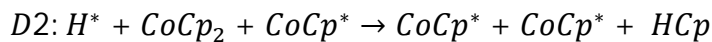
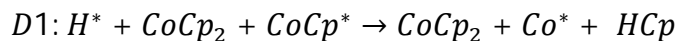
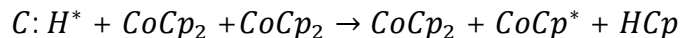


Figure 6. The configurations of two precursor CoCp_2 on NH_x -terminated (a) $\text{Co}(001)$ surface, and (b) $\text{Co}(100)$. The substrate Co atom is represented by orange. Carbon, nitrogen and hydrogen atoms are represented by grey, blue and white colour, respectively.

The preferred binding mode for two precursors is the same as for adsorption of a single precursor. On the $\text{Co}(001)$ surface, the upright adsorption mode is the most stable, while on the (100) surface the flat adsorption mode is the most stable. These adsorption modes are exothermic with computed adsorption energies of -1.63eV and -3.31eV , giving adsorption energies per precursor are -0.81eV and -1.65eV . Thus on the (001) surface, precursor adsorption is enhanced compared with adsorption of a single precursor (-0.68eV). In this adsorption configuration we see tilting of the two CoCp_2 precursors. Compared with adsorption of a single CoCp_2 on the $\text{Co}(100)$ surface, there is no difference in adsorption energy per precursor.

The further reaction of two precursor molecules of CoCp_2 on the NH_x terminated metal surfaces at ALD operating condition can proceed as follows:



Here, after the first hydrogen transfer, Reaction C, the second hydrogen transfer can result in two different by-products. Reaction D1 results in a Co atom and an intact adsorbed CoCp₂, while in reaction D2, two adsorbed CoCp fragments are present on the surface. The reaction energies of two precursor adsorption are with reference to the NH_x-terminated metal surface and two free CoCp₂. If one CpH molecule desorbs from the surface, the reaction energies are with reference to NH_x-terminated metal surface, two free CoCp₂, and free CpH. The reaction pathways are shown in Figure 7, with Reactions D1 and D2 shown in different colours and the calculated barriers for each hydrogen transfer step are presented in Table 6.

Table 6. The computed energy barriers for hydrogen transfer steps with respect to two metal precursors adsorption on NH_x terminated Co (001) and (100) surfaces at ALD conditions.

Computed Barriers/eV			
	$C: H^* + CoCp_2 + CoCp_2 \rightarrow$ $CoCp_2 + CoCp^* + HCp$	$D1: H^* + CoCp_2 + CoCp^* \rightarrow$ $CoCp_2 + Co^* + HCp$	$D2: H^* + CoCp_2 + CoCp^* \rightarrow$ $CoCp^* + CoCp^* + HCp$
Co(001)	0.74	1.18	0.75
Co(100)	No barrier	0.79	1.78

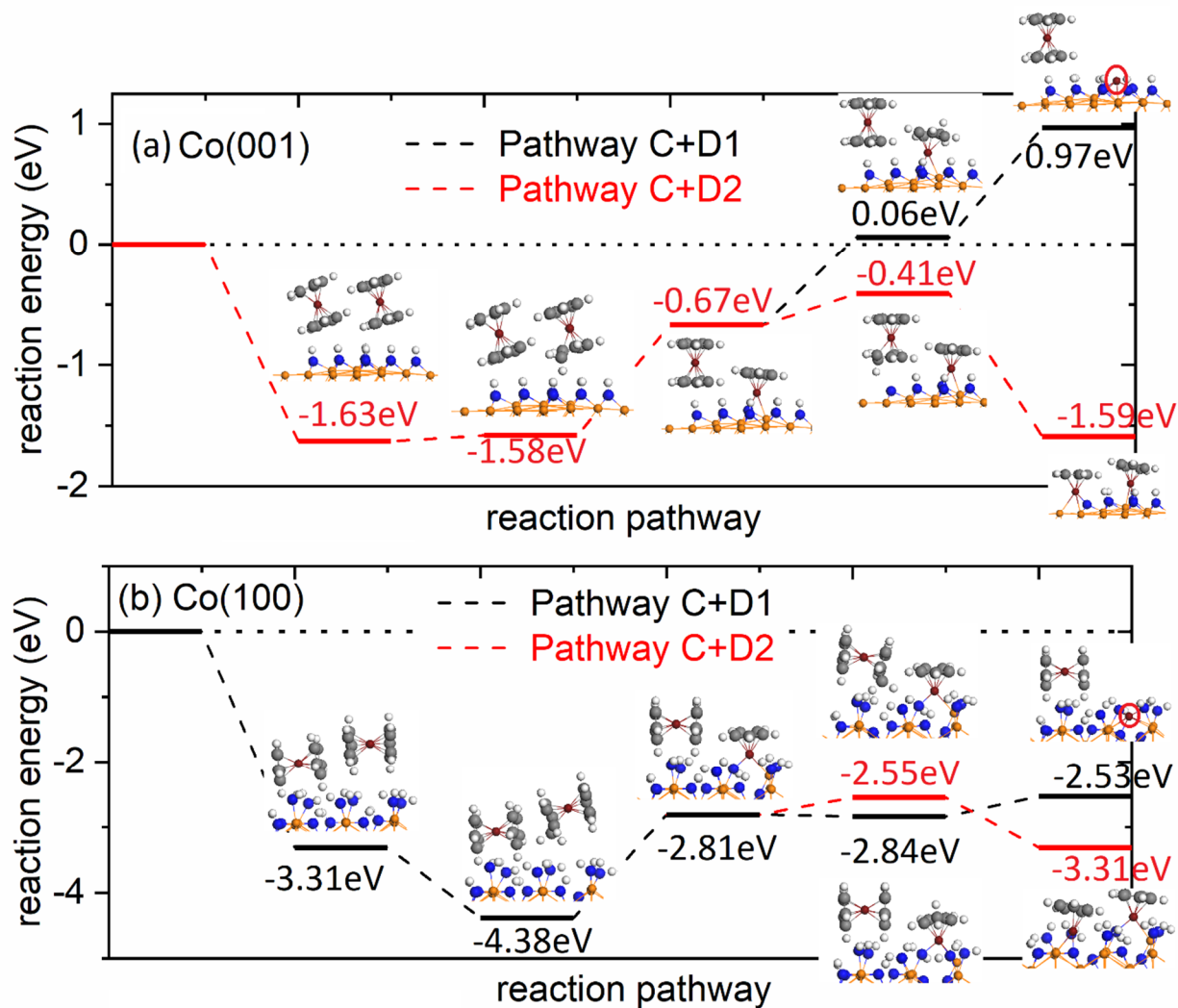


Figure 7. The CoCp₂ precursor reaction pathway on (a) Co(001) surface and (b) Co(100) surface for two CoCp₂ precursors. The black pathway is for reaction D1, resulting in a Co atom and adsorbed CoCp₂. The red pathway is for reaction D2, resulting in two CoCp fragments at the surface. The substrate Co atom is represented by orange colour and the Co atom from metal precursor CoCp₂ is represented by wine red colour. Carbon, nitrogen and hydrogen atoms are represented by grey, blue and white colour, respectively.

On the Co(001) surface, the first hydrogen transfer step is thermoneutral with a small energy change of 0.05eV and a moderate activation barrier of 0.74eV. This barrier is larger by 0.18 eV compared to the barrier for the first hydrogen transfer for a single CoCp₂ precursor. This indicates that a neighbouring precursor might slightly hinder the reactivity on the Co(001) surface.

After the desorption of fCpH, the elimination of the second Cp ligand for the same precursor, reaction D1, is unfavourable with an endothermic reaction energy and a high activation barrier of 1.18eV. The trend that formation of a bare Co atom is unfavourable on this surface persists with two CoCp₂ precursors.

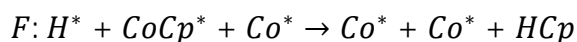
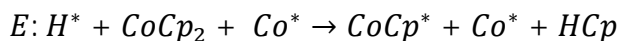
Alternatively, following reaction D2, the intact CoCp₂ precursor undergoes hydrogen transfer from the surface, with a moderate activation barrier of 0.75 eV, which is similar to that of reaction C. The elimination of the second Cp ligand is not favoured. Thus, with adsorption of multiple precursors, the final termination remains CoCp fragments on Co(001) surface.

On the Co(100) surface, the adsorption of two metal precursors is exothermic with a large energy gain of -3.31eV. As previously described, the channel H atom is more reactive than surface H atom. The first hydrogen transfer of the channel H atom is exothermic and is barrierless. Thus, a neighbouring CoCp₂ precursor promotes the first hydrogen transfer step by reducing the activation barrier from 0.52eV to no barrier on Co(100) surface.

After the desorption of this CpH, the elimination of the second Cp ligand from the same precursor as reaction C, indicated as reaction D1, with a computed activation barrier of 0.79eV, has a much lower activation barrier than the hydrogen transfer to a Cp ligand of the neighbouring CoCp₂ precursor, denoted as reaction D2, which has an activation barrier of 1.78eV. Thus, the elimination of two Cp ligands from one precursor is favoured rather than elimination from each precursor and

after two hydrogen transfer steps, the resulting structure is one Co atom deposited on the surface binding to N atom, and one intact CoCp₂ molecule.

After the elimination of two Cp ligands from a CoCp₂ precursor, we then further investigate hydrogen transfer and Cp elimination for the second CoCp₂ precursor, with the deposited Co on the Co(100) surface. The reactions are illustrated as follows:



The results are summarized in Figure 8. Again, the channel H atom is more reactive than the surface H atom. The first hydrogen transfer step is slightly endothermic, but still highly exothermic overall, with a moderate activation barrier of 0.89eV. After the desorption of first CpH, the second hydrogen transfer step is exothermic and has a moderate barrier of 0.75eV. After the second CpH desorption, two Co atoms are deposited on the surface.

The computed activation barriers for H transfer for a single CoCp₂ precursor, two surface bound CoCp₂ species, and one precursor with a bare Co atom Co + CoCp₂ on Co(100) surface are summarized in Table 7. We see that the activation barriers for Cp elimination via hydrogen transfer steps are all moderate and can be overcome at ALD operating condition and on this surface CpH elimination proceeds to leave Co atoms on the Co(100) surface. These Co atoms are bound to nitrogen atoms with Co-N distances of XXXXXX.

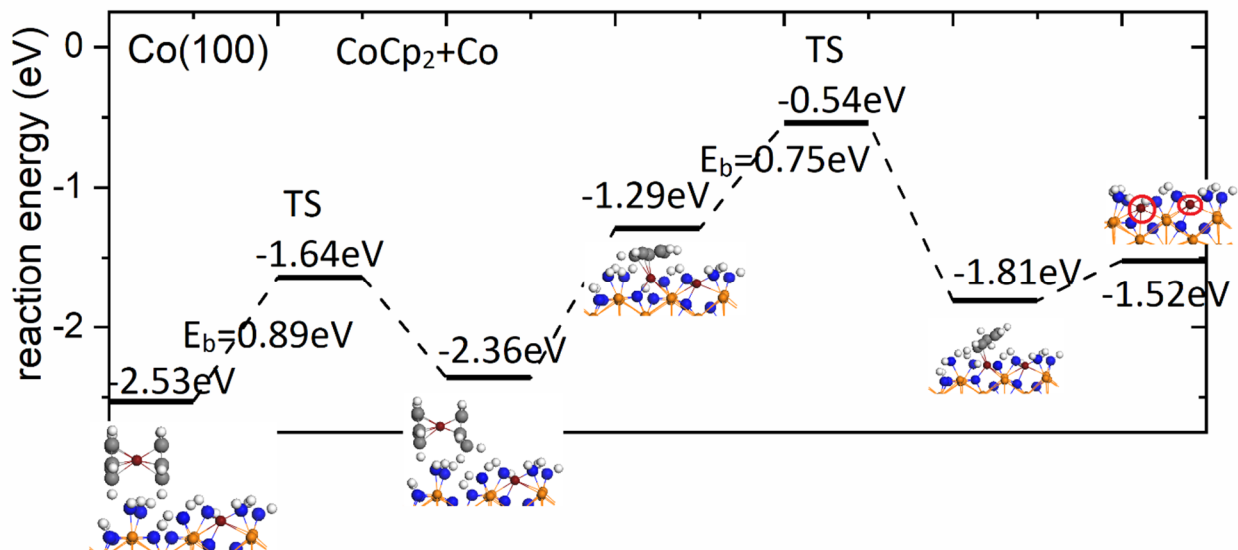


Figure 8. The plotted metal precursor reaction pathway on Co(100) surface with CoCp₂ reaction with one Co atom deposited on the surface. The substrate Co atom is represented by orange colour and the Co atom from metal precursor CoCp₂ is represented by wine red colour. Carbon, nitrogen and hydrogen atoms are represented by grey, blue and white colour, respectively.

Table 7. The calculated activation barriers for first and second hydrogen steps on NH_x-terminated Co(100) surface with one precursor CoCp₂, two precursors CoCp₂ + CoCp₂, and one precursor and one Co atom deposited on the surface Co + CoCp₂.

	Barriers/eV		
	CoCp ₂	CoCp ₂ + CoCp ₂	Co + CoCp ₂
1 st hydrogen transfer	0.52	No barrier	0.89
2 nd hydrogen transfer	0.85	0.79	0.75

3.4 Final structures after metal precursor pulse on Co (001) and (100) surfaces at ALD operating condition

Based on the discussion in section 3.3, on the Co(001) surface, the preferred termination is the CoCp fragment. With this in mind, we consider the saturation coverage of CoCp fragments on Co(001) to determine the maximum coverage of CoCp after the metal precursor pulse. The results are summarized in Figure 9. We see that at most three CoCp fragments can be adsorbed on NH_x -terminated Co(001) surface, which results in a coverage of 3.03 CoCp/nm^2 .

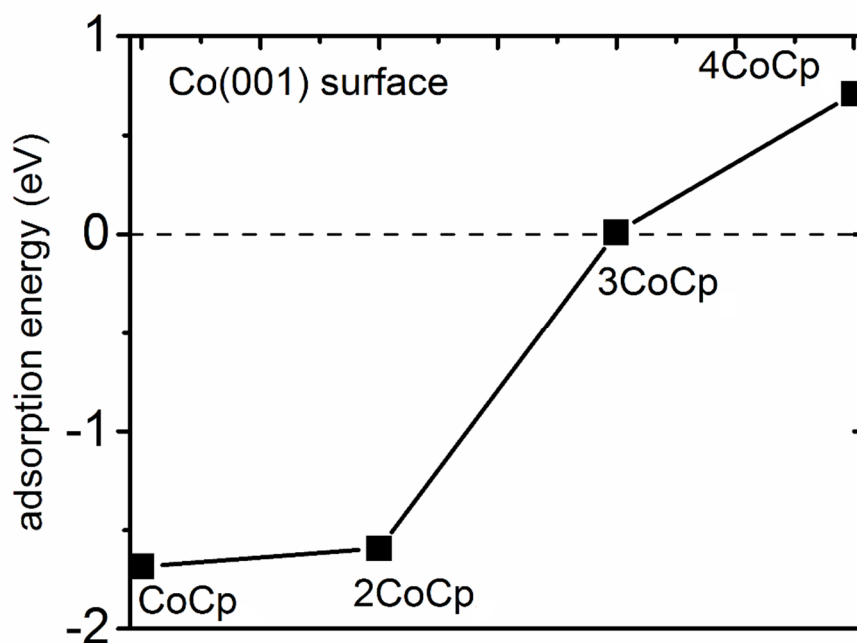


Figure 9. The adsorption energies of CoCp fragments on NH_x -terminated Co(001) surface at various coverages.

On the Co(100) surface, the channel hydrogen atoms are involved in the hydrogen transfer steps and the two Cp ligands are eliminated with hydrogen transfer, CpH formation and desorption. At ALD operating condition, the NH_x -termination is $6\text{NH} + 6\text{NH}_2$. In total, three Co atoms are

deposited on the surface. To explore if the surface H atoms can be consumed in the $\text{Co}(\text{Cp})_2$ pulse, we adsorb one CoCp_2 precursor on a structure in which all channel H atoms have been lost to study the energetics of hydrogen transfer via surface H from NH_2 . The calculated reaction pathway is shown in Figure 10.

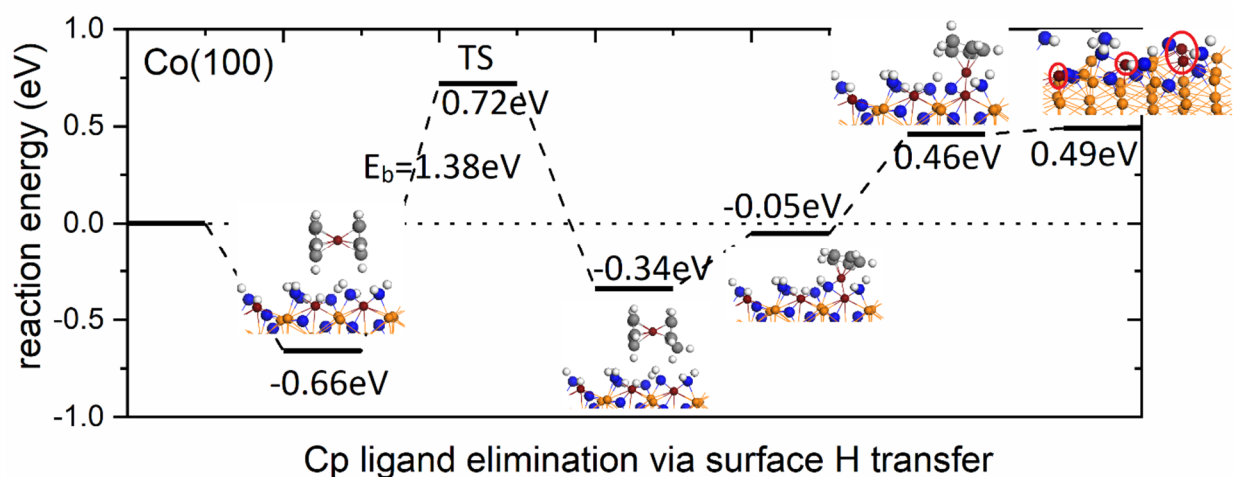


Figure 10. The plotted metal precursor reaction pathway on $\text{Co}(100)$ surface with Cp ligand elimination via surface hydrogen transfer. The substrate Co atom is represented by orange colour and the Co atom from metal precursor CoCp_2 is represented by wine red colour. Carbon, nitrogen and hydrogen atoms are represented by grey, blue and white colour, respectively.

With only surface H present, a CoCp_2 precursor has a moderate adsorption strength with a computed adsorption energy of -0.66eV . The first hydrogen transfer is endothermic by 0.32 eV and has a high barrier of 1.38eV . After desorption of CpH , the second hydrogen transfer is not favoured as the reaction energy is endothermic. Compared with channel hydrogen transfer, the Cp ligand elimination via surface hydrogen transfer is endothermic and has high activation barrier.

Thus, we concluded that the reaction will stop after all channel H atoms are consumed. The final structure on Co(100) surface shows Co atoms deposited on the surface with the coverage of 3.33 Co/nm². The final terminations after metal precursor pulse on Co (001) and (100) surfaces are shown in Figure 11. The reported growth rate of PE-ALD of Co using CoCp₂ and N-plasma varies from 0.26 Å/cycle to 0.97 Å/cycle.^{14, 17-18} Any remaining Cp ligands and NH_x species can be eliminated during the next N-plasma step.

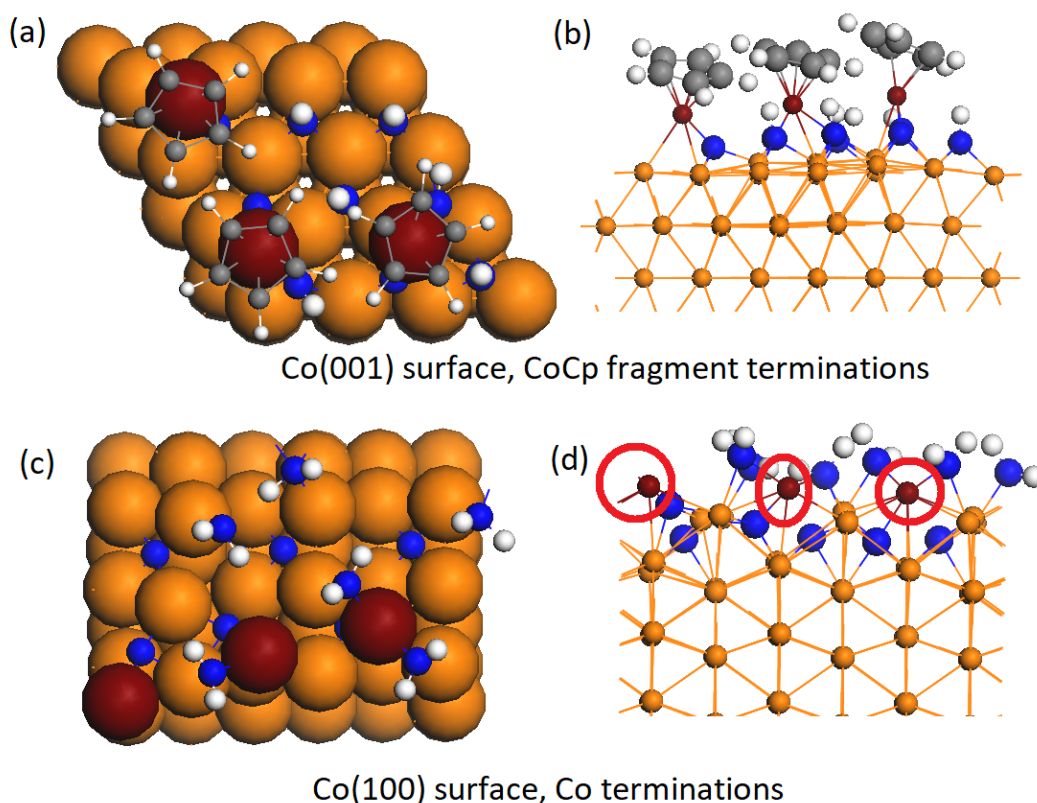


Figure 11. The configurations of final terminations after metal precursor pulse on Co(001) surface with (a) top view, and (b) side view, and Co(100) surface with (c) top view, and (d) side view. The substrate Co atom is represented by orange colour and the Co atom from metal precursor CoCp₂

is represented by wine red colour. Carbon, nitrogen and hydrogen atoms are represented by grey, blue and white colour, respectively.

4. Discussion

The deposition of Co thin film using a CoCp₂ precursor has been demonstrated experimentally.^{6, 18, 38-39} In plasma ALD studies, the co-reactants are NH₃ plasma or a mixture of N₂ and H₂ plasma. The reported growth per cycle (GPC) and Co thin film resistivity varies with operating temperature and co-reactants. For example, when the NH₃ plasma is used, at a deposition temperature of 300°C, the GPC and resistivity were 0.48 Å and 10 μΩcm, respectively.¹⁴ In another study with a co-reactant of N₂/H₂ plasma, the GPC was in the range of 0.26 Å to 0.65 Å for deposition temperatures in the range of 150°C to 450°C. The reported resistivity was 18 μΩcm.¹⁷ It was found that a small amount of N (*ca.* 2-3 at. %) was present in the deposited Co film when using NH₃ or mixture of N₂ and H₂ plasma. A slightly higher amount of N (*ca.* 4.5 at. %) is present in the subsurface region.¹⁸

In this paper, we start with NH_x-terminated Co surfaces from ref. 31. This is in accordance with the experimental conclusions that the NH_x species play an important role in the growth mechanism.^{18, 38-39} On a bare Co surface, the dissociation of CoCp₂ precursor is difficult as a result of the strong Co-C bond. On NH_x-terminated Co surfaces, the Cp ligand is eliminated via hydrogen transfer step and will desorb the surface as CpH. This is the key reaction mechanism during the metal precursor pulse.

From the calculation of activation barriers, the final surface termination on the Co(001) surface is CoCp fragments. The NH_x species are not fully eliminated during this step. On the Co(100)

surface, the two Cp ligands in CoCp_2 are eliminated and the final termination is Co-terminated NH_x -covered surface in which Co binds to surface N atom. On this surface, the preference is for the channel hydrogen to be removed, leaving NH_x species with surface hydrogen. These surface hydrogens are not reactive enough to promote CpH elimination.

When we consider multiple $\text{Co}(\text{Cp})_2$ precursors on the NH_x -terminated (100) and (001) surfaces, the reaction pathway is similar to that for a single precursor. On $\text{Co}(001)$, the preference is for CoCp species to be present, while on $\text{Co}(100)$, Cp is lost, leaving Co atoms bound to the surface. The simultaneous adsorption of two $\text{Co}(\text{Cp})_2$ precursors can promote the CpH elimination on the $\text{Co}(100)$ surface.

In the following N-plasma step, we expect that the surface CoCp fragment and surface terminating NH_x species are eliminated with plasma radicals such as N, H, NH and NH_2 . However, the channel N is difficult to remove completely. This is consistent with the experimental finding of subsurface N atoms in Co metal.^{18, 38-39}

The study of the plasma step is beyond the scope of this paper. However, we can explore some possible reactions of the surface bound NH_x species after CpH elimination on the $\text{Co}(100)$ surface, leading to the formation of N_2H_4 , NH_3 or N_2 . We discuss the results of possible surface reactions for the removal of surface NH_x species such as N_xH_y formation at the end of metal precursor pulse. For $\text{Co}(100)$, the two Cp ligands are removed completely via proton transfer and CpH formation and desorption. The channel H atoms are removed during the proton transfer step. The surface H atoms are not removed in this mechanism due to high proton transfer barrier. The coverage of deposited Co atoms on the surface is 3.33 Co/nm^2 . We consider N_2H_4 formation, NH formation, and H_2 formation and the results are summarized in Figure 12. The energies are discussed using

as reference the energy of final structure of Co deposited on NH_x -terminated $\text{Co}(100)$ surface as shown in Figure 12(a). After formation of N_2H_4 and relaxation, the resulting structure reverts to two NH_2 species terminating the surface, shown in Figure 12(b). NH formation and H_2 formation are both endothermic, with energy costs of 0.26eV for NH formation and 1.54eV for H_2 formation respectively, compared to original final structure. These are shown in Figure 12(c)-(d). Thus, surface reactions for the removal of surface NH_x species after the $\text{Co}(\text{Cp})_2$ precursor pulse are not favourable and the NH_x species will be removed in the following plasma step.

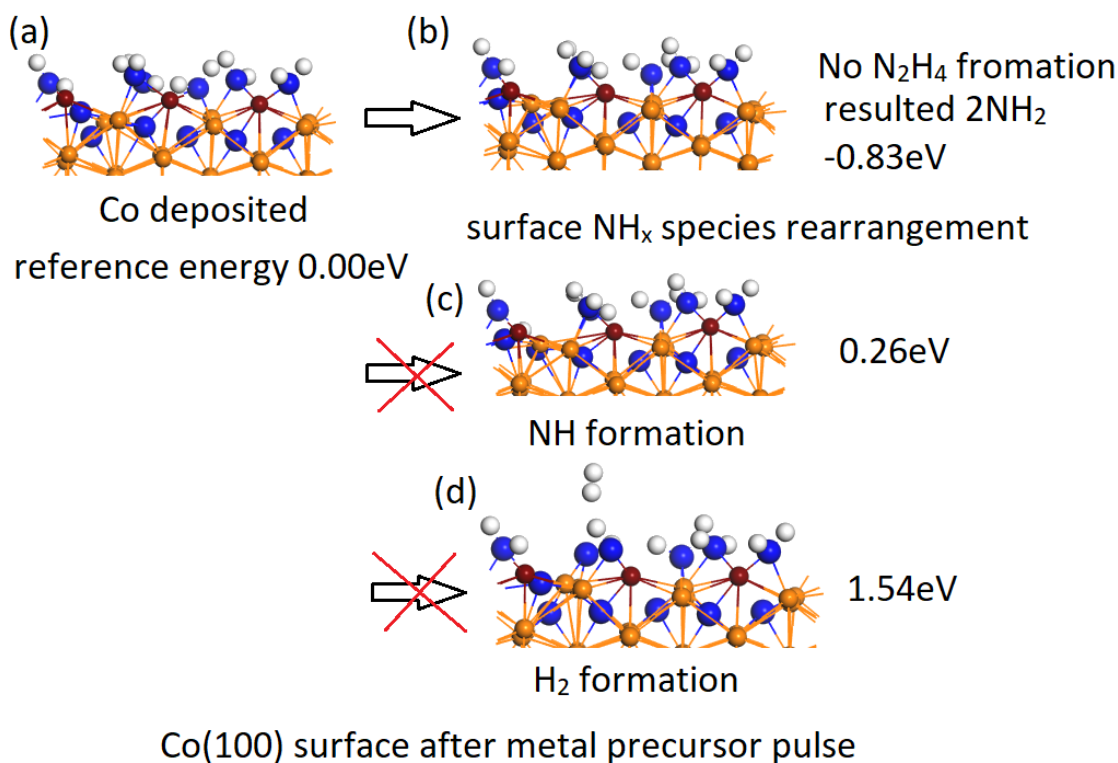


Figure 12. The configurations of surface reactions on $\text{Co}(100)$ surface including (a) original Co deposited on NH_x -terminated surface, (b) surface NH_x species rearrangement, (c) NH formation, and (d) H_2 formation.

5. Conclusions

When depositing metals, a non-oxidizing reactant is preferred because the O-source will cause contamination and oxidize the metal. The PE-ALD of Co using metal precursor and N-plasma has been demonstrated experimentally, but the reaction mechanism is not well-understood. After the N-plasma step, the resulted metal surfaces will be NH_x -terminated. The nature and stability of NH_x -terminated metal surfaces are studied in our previous published work.³¹ The present work focuses on the reaction mechanism during the metal precursor pulse on the NH_x -terminated surfaces. These final structures and terminations after metal precursor pulse are vital to model the following plasma pulse. The surface facets will result in different precursor adsorption orientation. CoCp_2 prefer up-right position with one Cp ring in close contact with NH_x -terminated (001) surface, while they are in flat position with both of the Cp rings anchored to zigzag channel on NH_x -terminated (100) surface.

The Cp ligands are eliminated via hydrogen transfer step and desorb from surface by forming CpH. The surface facet plays an important role in reaction energy and barriers for hydrogen transfer step. On the Co(001) surface, the NH_x termination is 0.56ML NH at ALD operating condition. With single CoCp_2 adsorption, only one Cp ligand is eliminated with moderate activation barrier at the value of 0.56eV. With two CoCp_2 adsorption, the neighbouring CoCp_2 has hindered the reactivity by increasing the barrier to 0.74eV. The final termination on NH_x -terminated Co(001) surface is CoCp fragments at the coverage of 3.03 CoCp/nm².

On the Co(100) surface, the NH_x termination is 0.67ML NH and 0.67ML NH_2 at ALD operating condition. Channel H atom is more reactive than surface H atom. With single CoCp_2 adsorption, the two Cp ligands are eliminated with moderate barriers at the value of 0.52eV and 0.85eV for the first and second hydrogen transfer. With two CoCp_2 adsorption, the neighbouring CoCp_2 has

promoted the reactivity by lowering the first hydrogen transfer barrier to no barrier and the second hydrogen transfer barrier to 0.79eV. After all channel H atoms are consumed, the Cp ligand elimination with surface H transfer has high barrier at the value of 1.38eV. The final termination on NH_x -terminated Co(100) is Co atoms deposited on the surface at the coverage of 3.33 Co/nm². During the following plasma step, the remaining Cp ligand (if any) and surface N atom are eliminated by N_xH_y radicals from the N-plasma (NH_3 or mixture of N_2 and H_2). After the plasma pulse, the metal surface will be NH_x -terminated and the whole system is ready for the next cycle. The reaction mechanism of N-plasma step is currently the subject of further study.

Acknowledgements

We acknowledge generous support from Science Foundation Ireland (SFI) through the SFI-NSFC Partnership program, Grant Number 17/NSFC/5279, NITRALD and National Natural Science Foundation of China, Grant number 51861135105. Computing resources have been generously supported by Science Foundation Ireland at Tyndall and through the SFI/HEA-funded Irish Centre for High End Computing (www.ichec.ie).

References

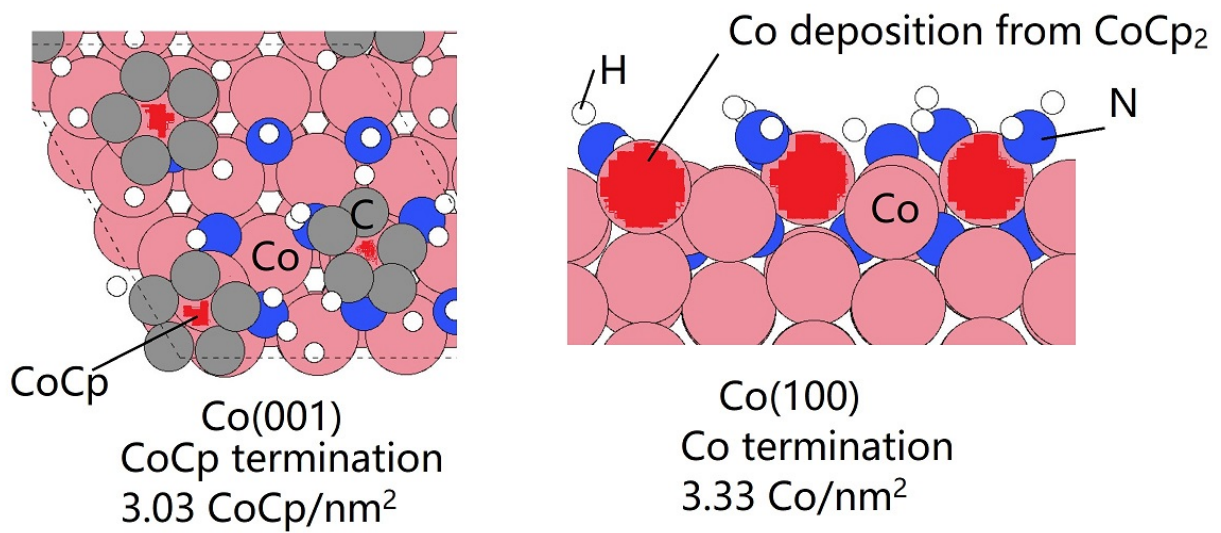
1. Tu, K., Recent advances on electromigration in very-large-scale-integration of interconnects. *J. Appl. Phys.* **2003**, 5451-5473.
2. Greenslit, D. V.; Eisenbraun, E., Characterization of Ultrathin PEALD-Grown RuCo Films for Diffusion Barrier and Copper Direct-Plate Applications. *ECS Trans.* **2011**, 35, 17-24.

3. Chakraborty, T.; Eisenbraun, E. T., Microstructure analysis of plasma enhanced atomic layer deposition-grown mixed-phase RuTa₂N barrier for seedless copper electrodeposition. *J. Vac. Sci. Technol. A* **2012**, *30*, 020604.
4. Miikkulainen, V.; Leskelä, M.; Ritala, M.; Puurunen, R. L., Crystallinity of inorganic films grown by atomic layer deposition: Overview and general trends. *J. Appl. Phys.* **2013**, *113*, 2.
5. Johnson, R. W.; Hultqvist, A.; Bent, S. F., A brief review of atomic layer deposition: from fundamentals to applications. *Mater. Today* **2014**, *17*, 236-246.
6. Kaloyeros, A. E.; Pan, Y.; Goff, J.; Arkles, B., Review—Cobalt Thin Films: Trends in Processing Technologies and Emerging Applications. *ECS J. Solid State Sci.* **2019**, *8*, P119-P152.
7. George, S. M., Atomic layer deposition: an overview. *Chem. Rev.* **2009**, *110*, 111-131.
8. Profijt, H.; Potts, S.; Van de Sanden, M.; Kessels, W., Plasma-assisted atomic layer deposition: basics, opportunities, and challenges. *J. Vac. Sci. Technol. A* **2011**, *29*, 050801.
9. Oviroh, P. O.; Akbarzadeh, R.; Pan, D.; Coetzee, R. A. M.; Jen, T. C., New development of atomic layer deposition: processes, methods and applications. *Sci. Technol. Adv. Mater.* **2019**, *20*, 465-496.
10. Kim, H., Atomic layer deposition of metal and nitride thin films: Current research efforts and applications for semiconductor device processing. *J. Vac. Sci. Technol. B* **2003**, *21*, 2231-2261.
11. Knisley, T. J.; Kalutarage, L. C.; Winter, C. H., Precursors and chemistry for the atomic layer deposition of metallic first row transition metal films. *Coord. Chem. Rev.* **2013**, *257*, 3222-3231.
12. Kim, H., Area selective atomic layer deposition of cobalt thin films. *ECS Trans.* **2008**, *16*, 219-225.
13. Lim, B. S.; Rahtu, A.; Gordon, R. G., Atomic layer deposition of transition metals. *Nat. Mater.* **2003**, *2*, 749.
14. Kim, H., High-quality cobalt thin films by plasma-enhanced atomic layer deposition. *Electrochem. Solid-State Lett.* **2006**, *9*, G323-G325.
15. Kim, K.; Lee, K.; Han, S.; Jeong, W.; Jeon, H., Characteristics of cobalt thin films deposited by remote plasma ALD method with dicobalt octacarbonyl. *J. Electrochem. Soc.* **2007**, *154*, H177-H181.
16. Zhu, B.; Ding, Z.-J.; Wu, X.; Liu, W.-J.; Zhang, D. W.; Ding, S.-J., Plasma-Enhanced Atomic Layer Deposition of Cobalt Films Using Co (EtCp)₂ as a Metal Precursor. *Nanoscale Res. Lett.* **2019**, *14*, 76.
17. Yoon, J.; Kim, D.; Cheon, T.; Kim, S.-H.; Kim, H., Atomic layer deposition of Co using N₂/H₂ plasma as a reactant. *J. Electrochem. Soc.* **2011**, *158*, H1179-H1182.
18. Vos, M. F.; van Straaten, G.; Kessels, W. E.; Mackus, A. J., Atomic Layer Deposition of Cobalt Using H₂-, N₂-, and NH₃-Based Plasmas: On the Role of the Co-reactant. *J. Phys. Chem. C* **2018**, *122*, 22519-22529.

19. Elliott, S. D., Atomic-scale simulation of ALD chemistry. *Semicond. Sci. Tech.* **2012**, *27*, 074008.
20. Phung, Q. M.; Pourtois, G.; Swerts, J.; Pierlout, K.; Delabie, A., Atomic Layer Deposition of Ruthenium on Ruthenium Surfaces: A Theoretical Study. *J. Phys. Chem. C* **2015**, *119*, 6592-6603.
21. Elliott, S. D.; Dey, G.; Maimaiti, Y., Classification of processes for the atomic layer deposition of metals based on mechanistic information from density functional theory calculations. *J. Chem. Phys.* **2017**, *146*, 052822.
22. Phung, Q. M.; Vancoillie, S.; Pourtois, G.; Swerts, J.; Pierlout, K.; Delabie, A., Atomic Layer Deposition of Ruthenium on a Titanium Nitride Surface: A Density Functional Theory Study. *J. Phys. Chem. C* **2013**, *117*, 19442-19453.
23. Fang, G.; Xu, L.; Cao, Y.; Li, A., Theoretical design and computational screening of precursors for atomic layer deposition. *Coord. Chem. Rev.* **2016**, *322*, 94-103.
24. Holme, T. P.; Prinz, F. B., Atomic Layer Deposition and Chemical Vapor Deposition Precursor Selection Method Application to Strontium and Barium Precursors. *J. Phys. Chem. A* **2007**, *111*, 8147-8151.
25. Puurunen, R. L., Surface chemistry of atomic layer deposition: A case study for the trimethylaluminum/water process. *J. Appl. Phys.* **2005**, *97*, 9.
26. Elliott, S.; Scarel, G.; Wiemer, C.; Fanciulli, M.; Pavia, G., Ozone-Based Atomic Layer Deposition of Alumina from TMA: Growth, Morphology, and Reaction Mechanism. *Chem. Mater.* **2006**, *18*, 3764-3773.
27. Langereis, E.; Bouman, M.; Keijmel, J.; Heil, S.; Van de Sanden, M.; Kessels, W., Plasma-assisted ALD of Al₂O₃ at low temperatures: reaction mechanisms and material properties. *ECS Trans.* **2008**, *16*, 247-255.
28. Rai, V. R.; Vandalon, V.; Agarwal, S., Surface reaction mechanisms during ozone and oxygen plasma assisted atomic layer deposition of aluminum oxide. *Langmuir* **2010**, *26*, 13732-13735.
29. Weckman, T.; Laasonen, K., First principles study of the atomic layer deposition of alumina by TMA-H₂O-process. *Phys. Chem. Chem. Phys.* **2015**, *17*, 17322-17334.
30. Elliott, S. D., Mechanism, Products, and Growth Rate of Atomic Layer Deposition of Noble Metals. *Langmuir* **2010**, *26*, 9179-9182.
31. Liu, J.; Nolan, M., Coverage and Stability of NH_x-Terminated Cobalt and Ruthenium Surfaces: A First-Principles Investigation. *J. Phys. Chem. C* **2019**, *123*, 25166-25175.
32. Kresse, G.; Joubert, D., From ultrasoft pseudopotentials to the projector augmented-wave method. *Phys. Rev. B* **1999**, *59*, 1758.

33. Perdew, J. P.; Chevary, J. A.; Vosko, S. H.; Jackson, K. A.; Pederson, M. R.; Singh, D. J.; Fiolhais, C., Atoms, molecules, solids, and surfaces: Applications of the generalized gradient approximation for exchange and correlation. *Phys. Rev. B* **1992**, *46*, 6671.
34. Perdew, J. P.; Burke, K.; Ernzerhof, M., Generalized gradient approximation made simple. *Phys. Rev. Lett.* **1996**, *77*, 3865.
35. Monkhorst, H. J.; Pack, J. D., Special points for Brillouin-zone integrations. *Phys. Rev. B* **1976**, *13*, 5188.
36. Maimaiti, Y.; Elliott, S. D., Precursor Adsorption on Copper Surfaces as the First Step during the Deposition of Copper: A Density Functional Study with van der Waals Correction. *J. Phys. Chem. C* **2015**, *119*, 9375-9385.
37. Henkelman, G.; Uberuaga, B. P.; Jónsson, H., A climbing image nudged elastic band method for finding saddle points and minimum energy paths. *J. Chem. Phys.* **2000**, *113*, 9901-9904.
38. Oh, I.-K.; Kim, H., Growth mechanism of Co thin films formed by plasma-enhanced atomic layer deposition using NH₃ as plasma reactant. *Current Applied Physics* **2017**, *17*, 333-338.
39. Reif, J.; Knaut, M.; Killge, S.; Winkler, F.; Albert, M.; Bartha, J. W., In vacuo studies on plasma-enhanced atomic layer deposition of cobalt thin films. *Journal of Vacuum Science & Technology A: Vacuum, Surfaces, and Films* **2020**, *38*, 012405.

Table of Contents Graphic



Final terminations after metal precursor CoCp₂ pulse